Inorganic–organic hybrid ionic liquid electrolytes for Na secondary batteries

Kazuhiko Matsumoto,[a,b,*,z] Ryosuke Taniki,[a] Toshiyuki Nohira,[a,b,c,*,z] Rika Hagiwara[a,b,*]

[a]Graduate School of Energy Science, Kyoto University, Yoshida, Sakyo−ku, Kyoto 606−8501, Japan

[b]Unit of Elements Strategy Initiative for Catalysts & Batteries (ESICB), Kyoto University, Katsura, Kyoto 615-8510, Japan

[c]Present address: Institute of Advanced Energy, Kyoto University, Uji 611-0011, Japan

*Electrochemical Society Active Member.

[z]Email: k-matsumoto@energy.kyoto-u.ac.jp (Kazuhiko Matsumoto),

nohira.toshiyuki.8r@kyoto-u.ac.jp (Toshiyuki Nohira), Tel: +81−75−753−5822, Fax: +81−75−753−5906

This was Paper 1472 presented at the Cancun, Mexico, Meeting of the Society, October 5–9, 2014.

Supplementary Information for publication is submitted with this manuscript.

Abstract

Sodium secondary batteries are attractive energy devices owing to the natural abundance of Na resources. The use of ionic liquid electrolytes can solve the safety problems associated with Na secondary batteries, especially for large-scale applications. The present study investigates the physical and the electrochemical properties of three inorganic–organic hybrid ionic liquid electrolytes for Na secondary batteries (Na[FSA]-[TMHA][FSA], Na[FSA]-[DBDM][FSA], and Na[FSA]-[AS(4.5)][FSA] (TMHA$^+$ = trimethylhexylammonium cation, DBDM$^+$ = dibutyldimethylammonium cation, AS(4.5)$^+$ = 5-azoniaspiro(4.5)nonane, and FSA$^-$ = bis(fluorosulfonyl)amide anion) have been investigated. In all the three systems, the liquid phase is observed at room temperature in a certain range of the Na[FSA] fraction. The ionic conductivities and the viscosities of the three systems obey the Vogel–Tammann–Fulcher equation, and the highest ionic conductivity among the three is observed for the Na[FSA]-[AS(4.5)][FSA] system. Their cathode limit on a Cu plate is Na metal deposition around 0 V vs. Na$^+$/Na and anode limit on a glassy carbon electrode is observed at ~5 V. The Coulombic efficiency of Na metal electrodeposition/dissolution is improved by elevation of temperature.

Introduction

Lithium secondary batteries are now widely utilized as energy storage devices in various applications such as portable electronics and automobiles.[1, 2] The high energy capacities and the high rate capabilities attained for state-of-the-art Li secondary batteries has enabled them to take the place of other types of secondary battery in many applications. However, the application of Li secondary batteries to large-scale energy storage encounters problems like high cost and uneven distribution of Li resources. Increasing number of researchers have studied the chemistry of Na secondary batteries,[3-7] targeting their future use as energy storage devices for stationary and transport purposes, owing to the high abundance and low cost of Na resources.[8, 9] The reasonably low Na^+/Na redox potential (-2.71 V vs. standard hydrogen electrode) also enables the construction of batteries with high energy densities.

Organic solutions containing $Na[ClO_4]$ or $Na[PF_6]$ are currently used as electrolytes in most Na secondary batteries.[10-12] Although such organic solutions have suitable ionic conductivities and electrochemical stabilities (e.g. 5.23 mS cm^{-1} for the highest ionic conductivity of the 0.8 M $Na[ClO_4]$-propylene carbonate solution),[10] practical applications are hindered by safety concerns, due to their high volatility and flammability. Ionic liquids are widely considered as possible replacements for organic electrolytes in the construction of safe electrochemical devices owing to their negligible vapor pressure, low flammability, and wide liquid-phase temperature range that negate the afore-mentioned safety concerns.[13]

In contrast to the extensive works on ionic liquid electrolytes for Li secondary batteries, reports on Na secondary batteries remain limited. The TFSA-based (TFSA = bis(trifluoromethylsulfonyl)amide)) ionic liquids give acceptable electrochemical performance when combined with alkali metal cations at intermediate temperatures,[14] and with the *N*-alkyl-*N*-methylpyrrolidinium cation at room temperature.[15-17] Ionic liquid electrolytes based on FSA⁻ (FSA⁻ = bis(fluorosulfonyl)amide)) reduce the lower limit of the liquid-phase temperature range and improve the ionic conductivity compared with TFSA-based ionic liquid electrolytes. Sodium secondary batteries utilizing the Na[FSA]-K[FSA] inorganic ionic liquid operates in the intermediate temperature range (above 353 K);[18-20] a further decrease in operation temperature was attained by introducing the organic ionic liquid, *N*-methyl-*N*-propylpyrrolidinium bis(fluorosulfonyl)amide ([C$_3$C$_1$pyrr][FSA]).[21, 22] Furthermore, the use of FSA⁻ enables stable electrodeposition/dissolution of Na metal with the 1-ethyl-3-methylimidazolium cation.[23] A similar benefit in the use of FSA⁻ against cathodic reactions was also observed in the Li secondary battery system.[24, 25]

Incorporation of other organic cations into ionic liquid electrolytes for Na secondary batteries is an interesting target, to enable the use of Na secondary batteries in a more diverse range of environments, such as at low and high temperatures. In the present study, three Na[FSA]-[Ocat][FSA]-type (Ocat⁺ = organic ammonium cation) inorganic–organic hybrid ionic liquid electrolytes, Na[FSA]-[TMHA][FSA], Na[FSA]-[DBDM][FSA], and Na[FSA]-[AS(4.5)][FSA] (TMHA⁺ = trimethylhexylammonium cation, DBDM⁺ = dibutyldimethylammonium cation, and AS(4.5)⁺ = 5-azoniaspiro[4.5]nonane), at different

x(Na[FSA]) (x(Na[FSA]) denotes mole fraction of Na[FSA]), are examined as electrolytes for Na secondary batteries. Their physical and electrochemical properties, such as phase transition, density, viscosity, ionic conductivity, electrochemical stability, and Na metal deposition/dissolution behavior, are investigated and discussed.

Experimental

General and Reagents.

Air-sensitive materials were handled in a glovebox under a dried and deoxygenated Ar atmosphere, or in an open dry chamber under a dried air atmosphere. The FSA salts, [TMHA][FSA] (Piotrek, purity > 99.9 %, water content < 50 ppm), [DBDM][FSA] (Piotrek, purity > 99.9 %, water content < 30 ppm), and Na[FSA] (Mitsubishi Materials Electronic Chemicals Co., Ltd., purity > 99.0 %, water content < 72 ppm) were purchased and vacuum-dried at 353 K prior to use. The [AS(4.5)]Br salt was prepared according to the previously reported method, from pyrrolidine (Aldrich, 99 %) and 1,5-dibromopentane (Aldrich, 97 %) in the presence of $K_2[CO_3]$.[26]

Synthesis of [AS(4.5)][FSA].

K[FSA] (Mitsubishi Materials Electronic Chemicals Co., Ltd., purity > 99.0 %), (15.7 g, 71.6 mmol) was added to a dichloromethane solution (~ 20 mL) of [AS(4.5)]Br (14.4 g, 65.4 mmol). The mixture was stirred overnight, and the resulting white precipitate of KBr was removed by filtration. The filtrate was washed with distilled water several times, until testing with 1 M aq.

AgNO$_3$ solution for the presence of residual bromide impurities in the water phase gave no precipitation of AgBr. The product was vacuum-dried at room temperature and then at 373 K (17.0 g, 53.1 mmol). Anal. Calcd. for C$_9$H$_{18}$N$_2$F$_2$S$_2$O$_4$: C, 33.75; H, 5.63; N, 8.75; F, 11.88; S, 20.02 (%). Found: C, 33.51; H, 5.63; N, 8.61; F, 12.02; S, 20.15 (%). Water content: 47 ppm.

Analysis.

Ionic conductivity was measured with the aid of an impedance analyzer (3532-80, Hioki E.E. Corp.) employing an AC impedance technique using a cell with stainless-steel disk electrodes. Viscosity was measured by a cone-and-plate rheometer (LVDV-II+PRO, Brookfield Engineering Laboratories, Inc.). Water content was measured by Karl-Fischer titration (899 Coulometer, Metrohm). Density was measured by a pycnometer method. Thermogravimetric (TG) and differential scanning calorimetric (DSC) analyses were performed under a dry Ar gas flow and at a scanning rate of 5 K min^{-1}, using Shimadzu DTG-60H (with an open Al cell) and Rigaku ThermoPlus EVO II DSC 8230 (with a sealed Al cell), respectively. Enthalpy changes were calculated by integrating the heat flow during each transition on the DSC curve, and entropy changes for the phase transitions were calculated by dividing the corresponding enthalpy changes by the transition temperatures. Elemental analysis was performed at Organic Elemental Analysis Research Center, Kyoto University.

Electrochemical measurements were performed on a Biologic VSP-300 system in the glovebox. Cyclic voltammetry was performed in a three-electrode cell using a Cu disk, an Al plate, or a glass-like carbon disk as the working electrode. Fresh Na metal (for reference and

counter electrodes) was cut into pieces and fixed on Ni mesh and were directly immersed in the

ionic liquid electrolyte containing Na[FSA]. The Na deposition/dissolution test was performed in

a two-electrode cell at a current density of 1.0 mA cm^{-2} using a Hokuto Denko HJ1001SD8

system. Sodium metal (0.08 C cm^{-2}) was first deposited on a Cu substrate with a surface area of

1.33 cm^2, and Na deposition/dissolution (0.02 C cm^{-2}) was repeated until the electrode potential

reached 0.5 V vs. Na/Na$^+$ during the dissolution. The average cycle efficiency of Na

deposition/dissolution (ε_{cycle}) is obtained according to the following equation (Equation 1):

$$\varepsilon_{cycle} = N_{eff} \cdot Q_{cycle} / (Q_{ex} + N_{eff} \cdot Q_{cycle}) \tag{1}$$

where N_{eff} is cycle number until the electrode potential reached 0.5 V vs. Na/Na$^+$, Q_{cycle} is the

electric charge for Na deposition/dissolution for one cycle (0.02 C cm^{-2}), and Q_{ex} is the extra

amount of electricity deposited before cycling (0.08 C cm^{-2}). Sodium metal was used as a counter

electrode.

Results and Discussion

Thermal behavior.

Table 1 summarizes thermal and physical properties of the inorganic-organic hybrid ionic

liquids studied in this work. As shown in the TG curves for [TMHA][FSA], [DBDM][FSA], and

[AS(4.5)][FSA] single salts at a scan rate of 5 K min^{-1} (Figure 1 (a)), all these salts start to exhibit

weight loss at ~ 470 K. The slight differences in the shapes of the TG curves suggest an order in

the thermal stability of [AS(4.5)][FSA] < [DBDM][FSA] < [TMHA][FSA]. The effects of the addition of Na[FSA] on the thermal stabilities of each salt were examined at x(Na[FSA]) = 0.5 (Figure 1 (b)). Weight loss commences for each salt at ~ 400 K. This loss is dominated by the decomposition of Na[FSA], because the weight loss for neat Na[FSA] also starts around 400 K under identical conditions. These results suggest that the decomposition temperature is determined by that of Na[FSA], even in the binary mixture of Na[FSA] and [Ocat][FSA]. According to a previous work for Li[FSA] in organic solutions, thermal stability is dependent on electrode materials, which should be also considered in the cases of ionic liquid electrolytes in view of practical applications.[27]

Figure 2 shows the phase diagrams for Na[FSA]-[TMHA][FSA], Na[FSA]-[DBDM][FSA], and Na[FSA]-[AS(4.5)][FSA] binary systems. It should be noted that these phase diagrams were constructed based on the DSC results (DSC curves are shown in Figures S1−S3, Supplementary Material) and do not represent the fully equilibrated states as discussed below. In all the cases, the liquidus line declines as x(Na[FSA]) in the binary systems increases from the neat [Ocat][FSA]. Even [TMHA][FSA] and [AS(4.5)][FSA], which are solid at room temperature in the neat form, have liquid phase at the room temperature range in a certain x(Na[FSA]) range. Such thermal behavior suggests that [Ocat][FSA] is not necessarily a room-temperature ionic liquid when mixed with Na[FSA]. In particular, the decrease of the liquidus temperature for the Na[FSA]-[AS(4.5)][FSA] system is remarkable (cf. melting point of the neat [AS(4.5)][FSA] is 409 K). In the Na[FSA]-rich region, the liquidus temperature increases with an increase in x(Na[FSA]) and the solid–solid phase transition of Na[FSA], which was observed in our previous

work,[28] is still observed for the Na[FSA]-[DBDM][FSA] and Na[FSA]-[AS(4.5)][FSA] systems. The solid–solid transition of [TMHA][FSA] is also observed in the x(Na[FSA])-poor region of the Na[FSA]-[TMHA][FSA] system. The glass transition temperature (T_g) increases with an increase in x(Na[FSA]), which correlates to the high viscosity of the Na[FSA]-rich region in the liquid state.[29] Crystallization disappears in a certain x(Na[FSA]) range, often referred to as the crystallinity gap, where only the glass transition is observed. For the previously reported ionic liquid systems based on Li[TFSA], disappearance of the crystalline phase was observed for organic cations such as 1-alkyl-3-methylimidazolium,[30] whereas the crystalline phase could be observed at any composition in the case of N-alkyl-N-methylpyrrolidinium.[31, 32] According to the DSC analysis of the Na[TFSA]-based ionic liquid systems (Na[TFSA]-[C$_2$C$_1$im][TFSA] and Na[TFSA]-[C$_4$C$_1$im][TFSA]), the crystallinity gap exists in certain composition ranges.[17] The FSA-based ionic liquid system, Li[FSA]-[C$_4$C$_1$pyrr][FSA], also exhibits a crystallinity gap in the Li[FSA]-rich region,[33] whereas the Li[FSA]-[C$_3$C$_1$pyrr][FSA] system give crystalline phases at the Li[FSA]: [C$_3$C$_1$pyrr][FSA] ratio of 0.06:0.94, 0.08:0.92, and 0.13:0.87.[34]

For salts which did not show crystallization during the DSC scan (x(Na[FSA]) = 0.3 and 0.4 for Na[FSA]-[TMHA][FSA], x(Na[FSA]) = 0.1, 0.2, and 0.3 for Na[FSA]-[DBDM][FSA], and x(Na[FSA]) = 0.4 and 0.5 for Na[FSA]-[AS(4.5)][FSA]), low-temperature thermal behavior was investigated by maintaining the salts at low temperatures to detect transitions which might have been missed by the DSC measurements. After storage at 243 K for four weeks, Na[FSA]-[TMHA][FSA] with x(Na[FSA]) of 0.3 partially froze and Na[FSA]-[AS(4.5)[FSA] with x(Na[FSA]) of 0.4 and 0.5 totally froze, whereas the other samples retained the liquid state,

suggesting that slow crystallization occurred in some cases. The Na[FSA]-[TMHA][FSA] with

x(Na[FSA]) of 0.3 and Na[FSA]-[AS(4.5)[FSA] with x(Na[FSA]) of 0.4 melted at around 283

and 298 K, respectively, whereas the Na[FSA]-[AS(4.5)][FSA] salt with x(Na[FSA]) of 0.5

partially retained the solid state, even at room temperature.

Viscosity and ionic conductivity

The viscosities, ionic conductivities, densities, and molar concentrations of the studied ionic

liquids are listed in Table 1. The molar concentrations of Na[FSA]-[TMHA][FSA],

Na[FSA]-[DBDM][FSA], and Na[FSA]-[AS(4.5)][FSA], respectively, are 1.421, 1.280, and

1.610 mol·L^{-1} at x(Na[FSA]) = 0.3. The Na[FSA]-[AS(4.5)][FSA] system exhibits a liquid phase

at room temperature even at a high Na[FSA] fraction, and gives a high molar concentration of

5.216 mol·L^{-1} for the salt at x(Na[FSA]) = 0.7. Such a high Na$^+$ concentration is one of the

fascinating features realized in ionic liquid systems, since the solubility of Na-salts is often

limited in organic solutions (c.f. 1.7 mol·L^{-1} for $NaClO_4$ in propylene carbonate). Figures 3 and 4

show the temperature dependence of viscosity and ionic conductivity for the

Na[FSA]-[Ocat][FSA] ionic liquids studied. Some of the viscosities and ionic conductivities were

measured in the supercooled state and are fitted by the Vogel-Tammann-Fulcher equations

(Equations (2) and (3) below). As is typical of ionic liquids,[35-37] they are described by concave

curves for viscosity and convex curves for ionic conductivity in the Arrhenius plots (Tables S1

and S2 for viscosity and ionic conductivity values, Supplementary Material).

$$\eta = A_\eta T^{1/2}\exp[B_\eta/(T-T_{0\eta})] \tag{2}$$

$$\sigma = A_\sigma T^{-1/2}\exp[-B_\sigma/(T-T_{0\sigma})] \tag{3}$$

where η and σ are viscosity and ionic conductivity, respectively, and A_η, B_η, $T_{0\eta}$, A_σ, B_σ, and $T_{0\sigma}$ are VTF parameters, as shown in Tables S3 and S4 (Supplementary Material). The viscosities and ionic conductivities increase and decrease, respectively, with an increase in x(Na[FSA]). In general, the ionic conductivities of ionic liquid electrolytes decrease with addition of Li and Na salts because of the increase in viscosity, [21, 38-40] and the present ionic liquid systems are no exceptions. Of these three ionic liquid electrolytes, the Na[FSA]-[AS(4.5)][FSA] system gives the lowest viscosity (171 mPa·s) and highest ionic conductivity (1.3 mS·cm^{-1}) at 298 K for x(Na[FSA]) = 0.3. Although the spiro-type cation usually gives a salt with a relatively high melting point,[41] organic solutions of it have high ionic conductivities.[42, 43] The restriction in motion of the pyrrolidinium and piperidinium rings may contribute to the high ionic conductivity, both in organic solutions and ionic liquids. Although the ionic conductivity of the Na[FSA]-[AS(4.5)][FSA] system (1.3 mS cm^{-1}) is lower than that of the Na[FSA]-[C$_3$C$_1$pyrr][FSA] (1.9 mS·cm^{-1})[22] and Na[FSA]-[C$_2$C$_1$im][FSA] (5.4 mS·cm^{-1})[23] systems at 298 K for x(Na[FSA]) = 0.3, it reaches a reasonably high value of 10 mS cm^{-1} at 358 K.

Electrochemical behavior

Figure 5 shows combined cyclic voltammograms of Cu disk (negative potential region), glass-like carbon disk (positive potential region), and Al plate (positive potential region) electrodes in the Na[FSA]-[TMHA][FSA], Na[FSA]-[DBDM][FSA], and Na[FSA]-[AS(4.5)][FSA] binary ionic liquids (x(Na[FSA]) = 0.3 at 298 K). During the scan in the negative direction on the Cu electrode in each ionic liquid, electrodeposition of Na metal is observed at a potential slightly lower than 0 V vs. Na$^+$/Na, due to the deposition overpotential. After reversing the direction of the potential scan, the corresponding electrodissolution of Na metal is observed. The Coulombic efficiencies (the ratio of the anodic and cathodic peak areas) for the Na metal deposition/dissolution based on these cyclic voltammograms are 36 % for Na[FSA]-[TMHA][FSA], 32 % for Na[FSA]-[DBDM][FSA], and 35 % for Na[FSA]-[AS(4.5)][FSA]. The low Coulombic efficiency is probably caused by the dendritic deposition of Na metal, which we visually confirmed. On the glass-like carbon electrode, the anodic current rises to ~ 5 V vs. Na$^+$/Na for each ionic liquid, which is similar to that previously reported for FSA-based ionic liquids.[21-23] It should be noted that the electrochemical stability of ionic liquid electrolytes is dependent on the electrode material and temperature.[44] For the Na[FSA]-[DBDM][FSA] ionic liquid, the anodic current reaches a limit, which may be caused by the formation of a passivation film consisting of the decomposition product from the cation. In contrast to the glass-like carbon electrode, little current is observed on the Al electrode during the positive scan, probably due to the formation of a passivation film on the electrode. This result demonstrates the validity of Al current collector for the positive electrode in Na secondary batteries using these ionic liquids.

Figure 6 shows the voltage profiles during Na deposition/dissolution tests in the Na[FSA]-[TMHA][FSA], Na[FSA]-[DBDM][FSA], and Na[FSA]-[AS(4.5)][FSA] binary ionic liquids (x(Na[FSA]) = 0.3, see Experimental section for the details of this test). The deposition/dissolution efficiencies, ε_{cycle}, defined by Equation (1) are 79 %, 67 %, and 71 % at 298 K for Na[FSA]-[TMHA][FSA], Na[FSA]-[DBDM][FSA], and Na[FSA]-[AS(4.5)][FSA], respectively. The elevation of temperature to 363 K improved the respective ε_{cycle} values to 92 %, 92 %, and 90 %. Chemical reaction of Na metal with a component species of the ionic liquids can be excluded, because such a reaction should be accelerated at high temperature, resulting in low Coulombic efficiencies. It is suggested that surface diffusion on metal becomes fast near the melting point of Na metal (371 K), leading to suppression of the dendritic deposition. Thus, Coulombic efficiencies are largely improved at 363 K. Formation of NaF layer at the surface of Na metal may also affect the high stability at high temperatures because such an effect was indicated for the electrolytes in Li secondary batteries.[45]

Conclusion

This paper reports physical and electrochemical properties of the three inorganic–organic hybrid ionic liquid electrolytes for Na secondary batteries (Na[FSA]-[TMHA][FSA], Na[FSA]-[DBDM][FSA], and Na[FSA]-[AS(4.5)][FSA]). As a result of a significant decrease in the liquidus temperature upon mixing of Na[FSA] and [Ocat][FSA], all three systems have a liquid phase at around room temperature in a certain range of x(Na[FSA]). The highest ionic conductivity in these systems was observed for [AS(4.5)][FSA] (1.3 mS·cm^{-1} at 298 K for

x(Na[FSA]) = 0.3). The wide electrochemical window and the high Coulombic efficiency of Na metal electrodeposition/dissolution, especially at elevated temperature, allow them to be utilized as electrolytes for Na secondary batteries.

Acknowledgement

References

1   M. Armand and J. M. Tarascon, *Nature* **451**, 652 (2008).
2   M. R. Palacin, *Chem. Soc. Rev.* **38**, 2565 (2009).
3   H. L. Pan, Y. S. Hu, and L. Q. Chen, *Energy Environ. Sci.* **6**, 2338 (2013).
4   S. W. Kim, D. H. Seo, X. H. Ma, G. Ceder, and K. Kang, *Adv. Energy. Mater.* **2**, 710 (2012).
5   M. D. Slater, D. Kim, E. Lee, and C. S. Johnson, *Adv. Funct. Mater.* **23**, 947 (2013).
6   V. Palomares, M. Casas-Cabanas, E. Castillo-Martinez, M. H. Han, and T. Rojo, *Energy Environ. Sci.* **6**, 2312 (2013).
7   K. B. Hueso, M. Armand, and T. Rojo, *Energy Environ. Sci.* **6**, 734 (2013).
8   S. R. Taylor and S. M. Mclennan, *Rev. Geophys.* **33**, 241 (1995).
9   Y. Nozaki, *Eos, Trans. Am. Geophys. Union* **78**, 221 (1997).
10   K. Kuratani, N. Uemura, H. Senoh, H. T. Takeshita, and T. Kiyobayashi, *J. Power Sources* **223**, 175 (2013).
11   A. Ponrouch, R. Dedryvere, D. Monti, A. E. Demet, J. M. A. Mba, L. Croguennec, C. Masquelier, P. Johansson, and M. R. Palacin, *Energy Environ. Sci.* **6**, 2361 (2013).
12   Z. L. Jian, W. Z. Han, X. Lu, H. X. Yang, Y. S. Hu, J. Zhou, Z. B. Zhou, J. Q. Li, W. Chen, D. F. Chen, and L. Q. Chen, *Adv. Energy. Mater.* **3**, 156 (2013).
13   H. Ohno, *Electrochemical Aspects of Ionic Liquids* (John Wiley & Sons Inc., Hoboken, New Jersey, 2011).
14   T. Nohira, T. Ishibashi, and R. Hagiwara, *J. Power Sources* **205**, 506 (2012).
15   S. A. M. Noor, P. C. Howlett, D. R. MacFarlane, and M. Forsyth, *Electrochim. Acta* **114**, 766 (2013).

16   L. G. Chagas, D. Buchholz, L. M. Wu, B. Vortmann, and S. Passerini, *J. Power Sources* **247**, 377 (2014).

17   D. Monti, E. Jonsson, M. R. Palacin, and P. Johansson, *J. Power Sources* **245**, 630 (2014).

18   K. Kubota, T. Nohira, T. Goto, and R. Hagiwara, *Electrochem. Commun.* **10**, 1886 (2008).

19   A. Fukunaga, T. Nohira, Y. Kozawa, R. Hagiwara, S. Sakai, K. Nitta, and S. Inazawa, *J. Power Sources* **209**, 52 (2012).

20   C. Y. Chen, K. Matsumoto, T. Nohira, R. Hagiwara, A. Fukunaga, S. Sakai, K. Nitta, and S. Inazawa, *J. Power Sources* **237**, 52 (2013).

21   C. S. Ding, T. Nohira, K. Kuroda, R. Hagiwara, A. Fukunaga, S. Sakai, K. Nitta, and S. Inazawa, *J. Power Sources* **238**, 296 (2013).

22   C. S. Ding, T. Nohira, R. Hagiwara, K. Matsumoto, Y. Okamoto, A. Fukunaga, S. Sakai, K. Nitta, and S. Inazawa, *J. Power Sources* **269**, 124 (2014).

23   K. Matsumoto, T. Hosokawa, T. Nohira, R. Hagiwara, A. Fukunaga, K. Numata, E. Itani, S. Sakai, K. Nitta, and S. Inazawa, *J. Power Sources* **265**, 36 (2014).

24   M. Ishikawa, T. Sugimoto, M. Kikuta, E. Ishiko, and M. Kono, *J. Power Sources* **162**, 658 (2006).

25   H. Matsumoto, H. Sakaebe, K. Tatsumi, M. Kikuta, E. Ishiko, and M. Kono, *J. Power Sources* **160**, 1308 (2006).

26   R. Taniki, K. Matsumoto, and R. Hagiwara, *Chem. Lett.* **42**, 1469 (2013).

27   G. G. Eshetu, S. Grugeon, G. Gachot, D. Mathiron, M. Armand, and S. Laruelle, *Electrochim. Acta* **102**, 133 (2013).

28   K. Matsumoto, T. Oka, T. Nohira, and R. Hagiwara, *Inorg. Chem.* **52**, 568 (2013).

29   W. Xu, E. I. Cooper, and C. A. Angell, *J. Phys. Chem. B* **107**, 6170 (2003).

30   Q. Zhou, K. Fitzgerald, P. D. Boyle, and W. A. Henderson, *Chem. Mater.* **22**, 1203 (2010).

31   W. A. Henderson and S. Passerini, *Chem. Mater.* **16**, 2881 (2004).

32   Q. Zhou, P. D. Boyle, L. Malpezzi, A. Mele, J. H. Shin, S. Passerini, and W. A. Henderson, *Chem. Mater.* **23**, 4331 (2011).

33   E. Paillard, Q. Zhou, W. A. Henderson, G. B. Appetecchi, M. Montanino, and S. Passerini, *J. Electrochem. Soc.* **156**, A891 (2009).

34   J. H. Huang and A. F. Hollenkamp, *J. Phys. Chem. C* **114**, 21840 (2010).

35   H. Vogel, *Phys. Z.* **22**, 645 (1921).

36   G. S. Fulcher, *J. Am. Ceram. Soc.* **8**, 339 (1925).

37   H. Tokuda, K. Hayamizu, K. Ishii, M. Abu Bin Hasan Susan, and M. Watanabe, *J. Phys. Chem. B* **108**, 16593 (2004).

38   A. I. Bhatt, A. S. Best, J. H. Huang, and A. F. Hollenkamp, *J. Electrochem. Soc.* **157**, A66 (2010).

39   J. Reiter, M. Nadherna, and R. Dominko, *J. Power Sources* **205**, 402 (2012).

40   S. Seki, Y. Ohno, Y. Kobayashi, H. Miyashiro, A. Usami, Y. Mita, H. Tokuda, M. Watanabe, K. Hayamizu, S. Tsuzuki, M. Hattori, and N. Terada, *J. Electrochem. Soc.* **154**, A173 (2007).

41   H. Matsumoto, N. Terasawa, H. Sakaebe, and S. Tsuzuki, US Patent, 20110070486 A1.

42   T. Devarajan, S. Higashiya, C. Dangler, M. Rane-Fondacaro, J. Snyder, and P. Haldar, *Electrochem. Commun.* **11**, 680 (2009).

43   X. W. Yu, D. B. Ruan, C. C. Wu, J. Wang, and Z. Q. Shi, *J. Power Sources* **265**, 309 (2014).

44   H. H. Zheng, J. H. Qin, Y. Zhao, T. Abe, and Z. Ogumi, *Solid State Ionics* **176**, 2219 (2005).

45   Y. Y. Lu, Z. Y. Tu, and L. A. Archer, *Nat. Mater.* **13**, 961 (2014).

Table 1 Selected physical properties of the Na[FSA]-[Ocat][FSA] ionic liquids[a]

Na[FSA]-[TMHA][FSA]

x(Na[FSA])	T_1 / K	T_2 / K	$T_{s\text{-}s}$ / K	T_g / K	ρ / g cm^{-3}	MC / mol L^{-1}	σ / mS cm^{-1}	η / mPa s
0.0	n.d.	324	n.d.	n.d.	–	–	–	–
0.1	278	321	n.d.	n.d.	–	–	1.9	95.8
0.2	282	305	n.d.	196	–	–	1.2	152
0.3	n.d.	n.d.	n.d.	199	1.364	1.421	0.75	234
0.4	n.d.	n.d.	n.d.	210	1.421	2.061	0.28	416
0.5	330	377	n.d.	211	–	–	–	–
0.6	326	379	n.d.	223	–	–	–	–
0.7	329	381	n.d.	248	–	–	–	–
0.8	328	385	n.d.	n.d.	–	–	–	–
0.9	329	388	n.d.	n.d.	–	–	–	–
1.0	n.d.	400	375	n.d.	–	–	–	–

Na[FSA]-[DBDM][FSA]

x(Na[FSA])	T_1 / K	T_2 / K	$T_{s\text{-}s}$ / K	T_g / K	ρ / g cm^{-3}	MC / mol L^{-1}	σ / mS cm^{-1}	η / mPa s
0.0	n.d.	288	n.d.	177	1.230	0	2.4	100
0.1	n.d.	n.d.	n.d.	181	1.264	0.361	1.6	141
0.2	n.d.	n.d.	n.d.	186	1.309	0.784	1.1	209
0.3	n.d.	n.d.	n.d.	195	1.354	1.280	0.69	356
0.4	n.d.	358	n.d.	204	–	–	–	–
0.5	317	388	n.d.	210	–	–	–	–
0.6	325	388	n.d.	222	–	–	–	–
0.7	325	395	375	230	–	–	–	–
0.8	333	396	374	243	–	–	–	–
0.9	333	397	374	252	–	–	–	–
1.0	n.d.	400	375	n.d.	–	–	–	–

Na[FSA]-[AS(4.5)][FSA]

x(Na[FSA])	T_1 / K	T_2 / K	$T_{s\text{-}s}$ / K	T_g / K	ρ / g cm^{-3}	MC / mol L^{-1}	σ / mS cm^{-1}	η / mPa s
0.0	n.d.	409	208 293 325	n.d.	–	–	–	–
0.1	n.d.	373	208 291 325	n.d.	–	–	–	–
0.2	263	326	204	n.d.	–	–	–	–

0.3	262	297	n.d.	197	1.531	1.610	1.3	171
0.4	n.d.	n.d.	n.d.	206	1.576	2.305	0.64	379
0.5	n.d.	n.d.	n.d.	216	1.638	3.129	0.31	709
0.6	n.d.	221	n.d.	219	1.703	4.087	0.12	2400
0.7	n.d.	330	n.d.	n.d.	1.776	5.216	0.036	7570
0.8	336	384	n.d.	n.d.	−	−	−	−
0.9	n.d.	396	377	n.d.	−	−	−	−
1.0	n.d.	400	375	197	−	−	−	−

[a] T_1: the onset temperature of melting, T_2: the end temperature of melting, $T_{s\text{-}s}$: solid-solid transition temperature, T_g: glass transition temperature, ρ: density at 298 K, MC: molar concentration at 298 K, σ: ionic conductivity at 298 K, η: viscosity at 298 K, and n.d.: not detected. The T_1, T_2, $T_{s\text{-}s}$, and T_g values were determined based on the DSC analysis at a scan rate of 5 K min^{-1}.

Figure captions

Figure 1 Thermogravimetric curves for the present FSA salts: (a) the neat [TMHA][FSA] (○), [DBDM][FSA] (△), and [AS(4.5)][FSA] (□) salts, (b) the mixtures at x(Na[FSA]) = 0.5 for Na[FSA]-[TMHA][FSA] (○), Na[FSA]-[DBDM][FSA] (△), and [AS(4.5)][FSA] (□). The data for neat Na[FSA] salt (▽) is also shown for comparison. The scan rate was 5 K min^{-1}.
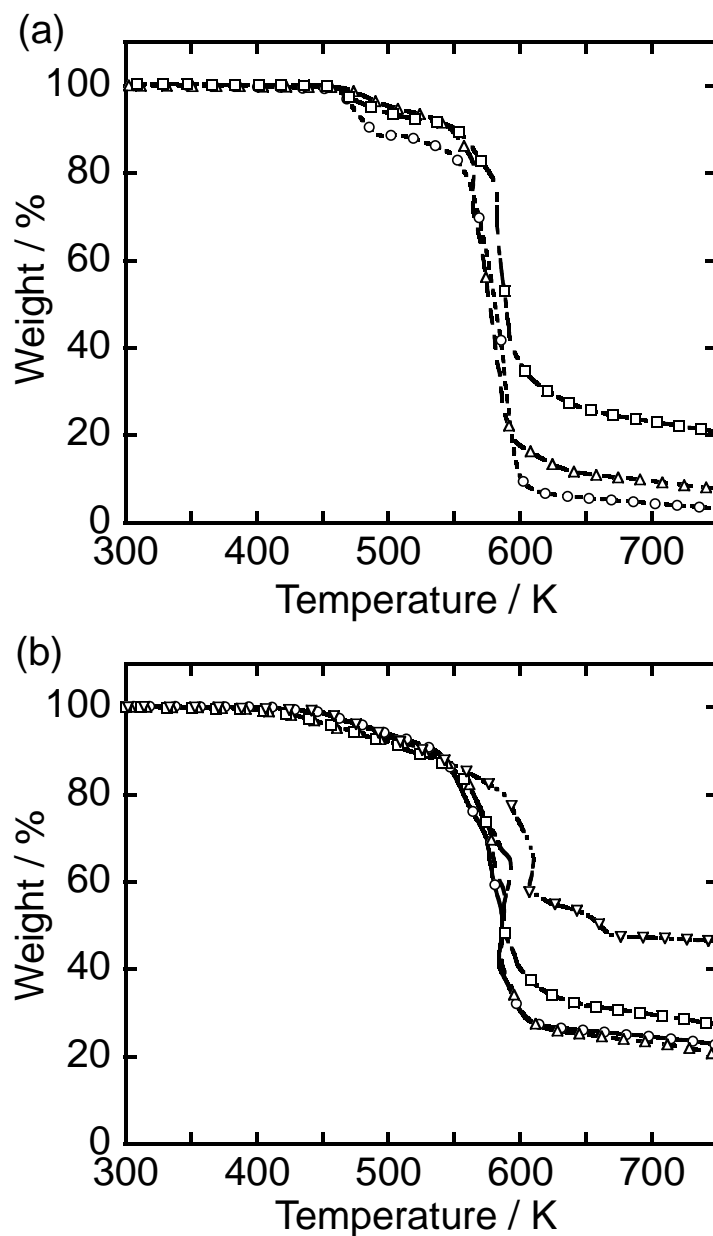
Figure 2 Phase diagrams of (a) Na[FSA]-[TMHA][FSA], (b) Na[FSA]-[DBDM][FSA], and (c) Na[FSA]-[AS(4.5)][FSA] systems based on the DSC transition temperatures in Table 1 (●: the onset temperature of melting (T_1), ◆: the end temperature of melting (T_2): ■: the solid-solid transition temperature (T_{s-s}), and ▲: glass transition temperature (T_g)).

Figure 3 Arrhenius plots of viscosity for the (a) Na[FSA]-[TMHA][FSA] (x(Na[FSA]) = 0.0 − 0.4) ionic liquids, (b) Na[FSA]-[DBDM][FSA] (x(Na[FSA]) = 0.0 − 0.3), and (c) Na[FSA]-[AS(4.5)][FSA] (x(Na[FSA]) = 0.3 − 0.7). ●: x(Na[FSA]) = 0.0, ■: x(Na[FSA]) = 0.1, ▲: x(Na[FSA]) = 0.2, ◆: x(Na[FSA]) = 0.3, ▼: x(Na[FSA]) = 0.4, +: x(Na[FSA]) = 0.5, ○: x(Na[FSA]) = 0.6, and □: x(Na[FSA]) = 0.7.
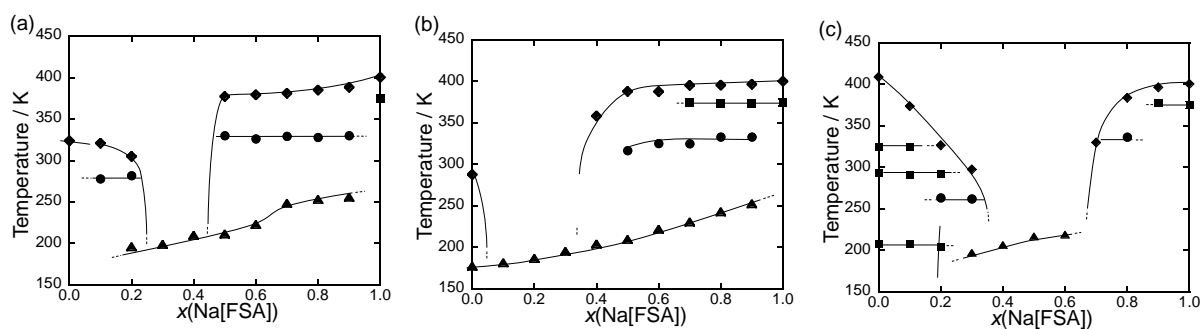
Figure 4 Arrhenius plots of ionic conductivity for the (a) Na[FSA]-[TMHA][FSA] (x(Na[FSA]) = 0.0 − 0.4) ionic liquids, (b) Na[FSA]-[DBDM][FSA] (x(Na[FSA]) = 0.0 − 0.3), and (c) Na[FSA]-[AS(4.5)][FSA] (x(Na[FSA]) = 0.3 − 0.7). ●: x(Na[FSA]) = 0.0, ■: x(Na[FSA]) = 0.1, ▲: x(Na[FSA]) = 0.2, ◆: x(Na[FSA]) = 0.3, ▼: x(Na[FSA]) = 0.4, +: x(Na[FSA]) = 0.5, ○: x(Na[FSA]) = 0.6, and □: x(Na[FSA]) = 0.7.

Figure 5 Combined cyclic voltammograms of Cu disk (negative potential region), glass-like carbon (GC) disk (positive potential region), and Al plate (positive potential region) electrodes in the (a) Na[FSA]-[TMHA][FSA], (b) Na[FSA]-[DBDM][FSA], and (c) Na[FSA]-[AS(4.5)][FSA] ionic liquids at x(Na[FSA]) = 0.3. Reference and counter electrodes are Na metal. Temperature: 298 K and scan rate: 5 mV s^{-1}.
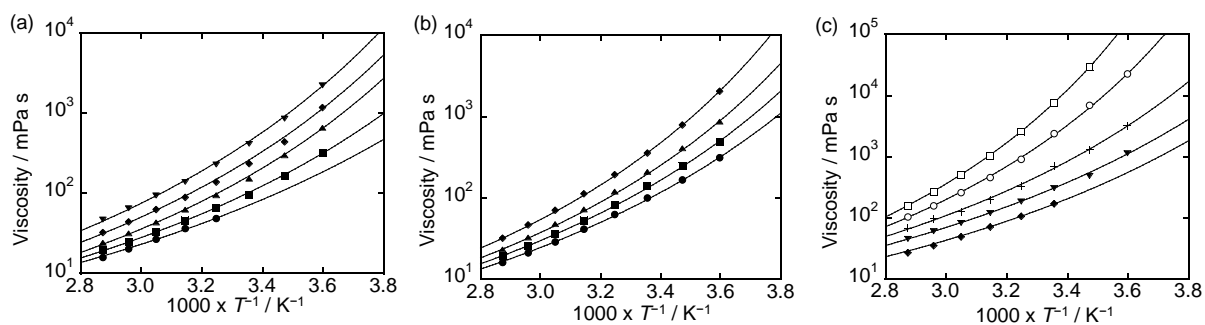
Figure 6 Voltage profile during Na metal deposition/dissolution tests for Na[FSA]-[TMHA][FSA] ((a) at 298 K and (d) at 363 K), Na[FSA]-[DBDM][FSA] ((b) at 298 K and (e) at 363 K), and Na[FSA]-[AS(4.5)][FSA] ((c) at 298 K and (f) 363 K) ionic liquids at x(Na[FSA]) = 0.3. A Cu plate was used as a working electrode. Sodium metal of 0.08 C cm^{-2} was first deposited on a Cu substrate and Na deposition and dissolution of 0.02 C cm^{-2} were repeated until the electrode potential reached 0.5 V vs. Na/Na$^+$ during the dissolution (see Experimental section for the details of this test). The current density was 0.1 (or −0.1) mA cm^{-2} through the test.
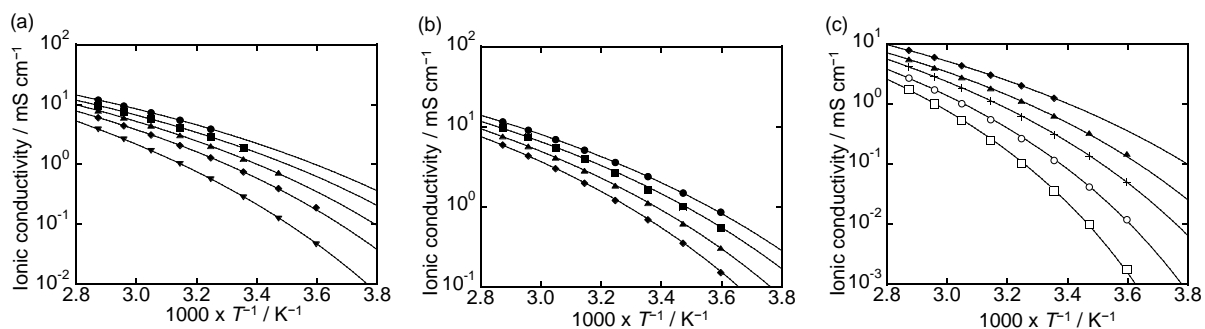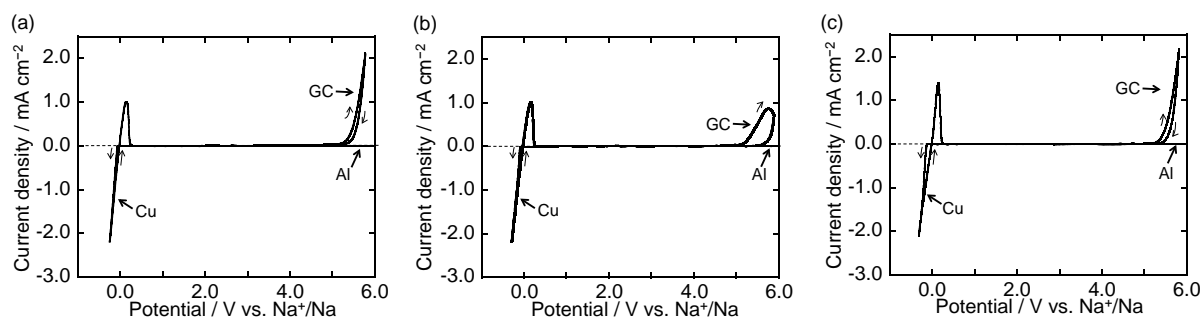
Figure 1 Thermogravimetric curves for the present FSA salts: (a) the neat [TMHA][FSA] (○), [DBDM][FSA] (△), and [AS(4.5)][FSA] (□) salts, (b) the mixtures at x(Na[FSA]) = 0.5 for Na[FSA]-[TMHA][FSA] (○), Na[FSA]-[DBDM][FSA] (△), and [AS(4.5)][FSA] (□). The data for neat Na[FSA] salt (▽) is also shown for comparison. The scan rate was 5 K min^{-1}.

Figure 2 Phase diagrams of (a) Na[FSA]-[TMHA][FSA], (b) Na[FSA]-[DBDM][FSA], and (c) Na[FSA]-[AS(4.5)][FSA] systems based on the DSC transition temperatures in Table 1 (●: the onset temperature of melting (T_1), ◆: the end temperature of melting (T_2): ■: the solid-solid transition temperature (T_{s-s}), and ▲: glass transition temperature (T_g)).

Figure 3 Arrhenius plots of viscosity for the (a) Na[FSA]-[TMHA][FSA] (x(Na[FSA]) = 0.0 − 0.4) ionic liquids, (b) Na[FSA]-[DBDM][FSA] (x(Na[FSA]) = 0.0 − 0.3), and (c) Na[FSA]-[AS(4.5)][FSA] (x(Na[FSA]) = 0.3 − 0.7). ●: x(Na[FSA]) = 0.0, ■: x(Na[FSA]) = 0.1, ▲: x(Na[FSA]) = 0.2, ◆: x(Na[FSA]) = 0.3, ▼: x(Na[FSA]) = 0.4, +: x(Na[FSA]) = 0.5, ○: x(Na[FSA]) = 0.6, and □: x(Na[FSA]) = 0.7.
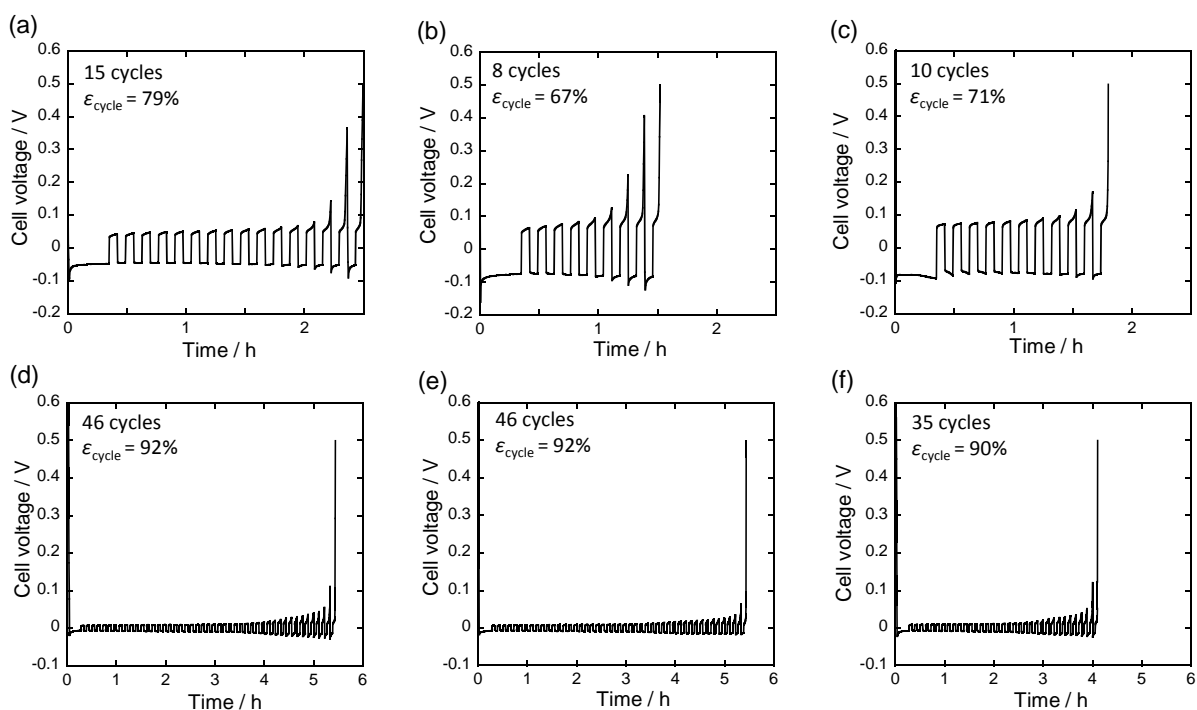
Figure 4 Arrhenius plots of ionic conductivity for the (a) Na[FSA]-[TMHA][FSA] (x(Na[FSA]) = 0.0 − 0.4) ionic liquids, (b) Na[FSA]-[DBDM][FSA] (x(Na[FSA]) = 0.0 − 0.3), and (c) Na[FSA]-[AS(4.5)][FSA] (x(Na[FSA]) = 0.3 − 0.7). ●: x(Na[FSA]) = 0.0, ■: x(Na[FSA]) = 0.1, ▲: x(Na[FSA]) = 0.2, ◆: x(Na[FSA]) = 0.3, ▼: x(Na[FSA]) = 0.4, +: x(Na[FSA]) = 0.5, ○: x(Na[FSA]) = 0.6, and □: x(Na[FSA]) = 0.7.

Figure 5 Combined cyclic voltammograms of Cu disk (negative potential region), glass-like carbon (GC) disk (positive potential region), and Al plate (positive potential region) electrodes in the (a) Na[FSA]-[TMHA][FSA], (b) Na[FSA]-[DBDM][FSA], and (c) Na[FSA]-[AS(4.5)][FSA] ionic liquids at x(Na[FSA]) = 0.3. Reference and counter electrodes are Na metal. Temperature: 298 K and scan rate: 5 mV s^{-1}.

Figure 6 Voltage profile during Na metal deposition/dissolution tests for Na[FSA]-[TMHA][FSA] ((a) at 298 K and (d) at 363 K), Na[FSA]-[DBDM][FSA] ((b) at 298 K and (e) at 363 K), and Na[FSA]-[AS(4.5)][FSA] ((c) at 298 K and (f) 363 K) ionic liquids at x(Na[FSA]) = 0.3. A Cu plate was used as a working electrode. Sodium metal of 0.08 C cm^{-2} was first deposited on a Cu substrate and Na deposition and dissolution of 0.02 C cm^{-2} were repeated until the electrode potential reached 0.5 V vs. Na/Na$^+$ during the dissolution. The current density was 0.1 (or −0.1) mA cm^{-2} through the test.